



LAWRENCE
LIVERMORE
NATIONAL
LABORATORY

Capsule Performance Optimization in the National Ignition Campaign

O. L. Landen, T. R. Boehly, D. K. Bradley, D. G. Braun, D. A. Callahan, P. M. Celliers, G. W. Collins, E. L. Dewald, L. Divol, S. H. Glenzer, A. Hamza, D. G. Hicks, N. Hoffman, N. Izumi, O. S. Jones, R. K. Kirkwood, G. A. Kyrala, P. Michel, J. Milovich, D. H. Munro, R. E. Olson, A. Nikroo, H. F. Robey, B. K. Spears, C. A. Thomas, S. V. Weber, D. C. Wilson, M. M. Marinak, L. J. Suter, B. A. Hammel, D. D. Meyerhofer, J. Atherton, J. Edwards, S. W. Haan, J. D. Lindl, B. J. MacGowan, E. I. Moses

November 30, 2009

Division of Plasma Physics Meeting 2009
Atlanta, GA, United States
November 1, 2009 through November 6, 2009

Disclaimer

This document was prepared as an account of work sponsored by an agency of the United States government. Neither the United States government nor Lawrence Livermore National Security, LLC, nor any of their employees makes any warranty, expressed or implied, or assumes any legal liability or responsibility for the accuracy, completeness, or usefulness of any information, apparatus, product, or process disclosed, or represents that its use would not infringe privately owned rights. Reference herein to any specific commercial product, process, or service by trade name, trademark, manufacturer, or otherwise does not necessarily constitute or imply its endorsement, recommendation, or favoring by the United States government or Lawrence Livermore National Security, LLC. The views and opinions of authors expressed herein do not necessarily state or reflect those of the United States government or Lawrence Livermore National Security, LLC, and shall not be used for advertising or product endorsement purposes.

Capsule Performance Optimization in the National Ignition Campaign*

O. L. Landen¹, T. R. Boehly², D. K. Bradley¹, D. G. Braun¹, D. A. Callahan¹, P. M. Celliers¹,
G. W. Collins¹, E. L. Dewald¹, L. Divol¹, S. H. Glenzer¹, A. Hamza¹, D. G. Hicks¹, N.
Hoffman³, N. Izumi¹, O. S. Jones¹, R. K. Kirkwood¹, G. A. Kyrala³, P. Michel¹, J. Milovich¹,
D. H. Munro¹, R. E. Olson⁴, A. Nikroo⁵, H. F. Robey¹, B. K. Spears¹, C. A. Thomas¹, S. V.
Weber¹, D. C. Wilson³, M. M. Marinak¹, L. J. Suter¹, B. A. Hammel¹, D. D. Meyerhofer², J.
Atherton¹, J. Edwards¹, S.W. Haan¹, J. D. Lindl¹, B. J. MacGowan¹, and E.I. Moses¹

¹Lawrence Livermore National Laboratory, Livermore, CA, 94550, USA

²Laboratory for Laser Energetics, Rochester, NY, USA

³Los Alamos National Laboratory, Los Alamos, NM, USA

⁴Sandia National Laboratory, Albuquerque, NM, USA

⁵General Atomics, San Diego, CA, USA

Abstract

A capsule performance optimization campaign will be conducted at the National Ignition Facility [1] to substantially increase the probability of ignition by laser-driven hohlraums [2]. The campaign will experimentally correct for residual uncertainties in the implosion and hohlraum physics used in our radiation-hydrodynamic computational models before proceeding to cryogenic-layered implosions and ignition attempts. The required tuning techniques using a variety of ignition capsule surrogates have been demonstrated at the Omega facility under scaled hohlraum and capsule conditions relevant to the ignition design and shown to meet the required sensitivity and accuracy. In addition, a roll-up of all expected

random and systematic uncertainties in setting the key ignition laser and target parameters due to residual measurement, calibration, cross-coupling, surrogacy, and scale-up errors has been derived that meets the required budget.

*This work was performed under the auspices of the U.S. Department of Energy by Lawrence Livermore National Laboratory under Contract DE-AC52-07NA27344.

INTRODUCTION

The overall goal of the capsule performance optimization campaign is to empirically correct for residual uncertainties in the implosion and hohlraum physics used in our radiation-hydrodynamic computational models [3,4] before proceeding to cryogenic-layered implosions [5] and ignition attempts. This will be accomplished using a variety of surrogate targets that will set key laser, hohlraum and capsule parameters to maximize ignition capsule implosion velocity, while minimizing fuel entropy (or adiabat), core shape asymmetry and ablator-fuel mix. This is followed by intentionally-dudged tritium-rich but deuterium-poor cryo-layered implosions to check the efficacy of the tuning through shared observables such as core symmetry and bangtime, and from implosion performance. Finally, if the chosen ignition design called for larger scale, the tuning would be checked at this scale, before proceeding to tests of alpha-heating and ignition.

Extensive computational multivariable sensitivity studies [6] have shown that, the probability of ignition is well correlated to the four key implosion parameters of 1D peak fuel implosion velocity v , 1D burn-averaged imploded fuel adiabat a , rms asymmetry $\Delta R_{\text{hotspot}}/R_{\text{hotspot}}$ at the hotspot-main fuel interface, and fraction $\Delta R_{\text{mix}}/\Delta R_{\text{fuel}}$ of fuel mixed with ablator. The fuel adiabat is defined as the ratio of the ion + electron pressure to the electron Fermi pressure at zero temperature. The product of power laws of these four parameters, for small excursions, can be used to define an Ignition Threshold Factor (ITF) given by the following equation:

$$\text{ITF} = \frac{E_{fuel}}{3.2kJ} \left(\frac{v}{380km/sec} \right)^{5.9} \left(\frac{\alpha}{1.46} \right)^{-3.9} \left(1 - \frac{\Delta R_{hotspot}}{R_{hotspot}} \right)^{3.5} \left(1 - \frac{0.5\Delta R_{mix}}{\Delta R_{fuel}} \right)$$

The constants 380 km/s and 1.46 in the denominators are specific to the particular 285 eV 1.2 MJ Be design [7] considered here that culminates in 3.2 kJ of stored capsule fuel energy. An ITF of 1 equates to 50% probability of ignition. Tuning is expected to increase the mean ITF from ≈ 0.2 to ≈ 1.5 , with ITF widths of ≈ 0.2 and ≈ 0.5 as set by the target physics models uncertainties, and by the quadrature sum of expected residual shot-to-shot variability in laser and target parameters and residual errors in tuning, respectively.

The expected initial and final uncertainties in the four implosion parameters are given in the second and third columns in Table I. The initial uncertainties have been estimated based on a combination of level of confidence in extrapolating radiation hydrodynamics models fitting Nova, Omega and Z facility hohlraum energetics, x-ray driven planar hydrodynamics and gas-filled hohlraum implosions data and residual differences between EOS, opacity and conductivity models for the hohlraum, ablator and DT fuel plasmas. These uncertainties translate to uncertainties in capsule ablation rate affecting implosion velocities, to uncertainties in hohlraum x-ray conversion efficiency, albedo and radiation hydrodynamics affecting drive symmetry, and to uncertainties in hard x-ray preheat levels, ablator compressibility and dopant opacity affecting fuel adiabats through shock transit times, and affecting level of ablator-fuel mix through the ablator-fuel interface Atwood number.

The tuning campaign is based on the principal that these physics uncertainties can be empirically corrected for by adjusting key laser and target parameters around their nominal

values, thereby increasing the ITF by increasing implosion velocity, and lowering fuel adiabat, asymmetry and mix. 16 principal adjustable parameters have been identified, schematically shown in Figure 1 and listed in the fourth column in Table I alongside the implosion parameter they affect. For the laser, they are the power levels for the 5 phases in the laser pulse, the launch time for the second, third and fourth steps, the end-point in the 4th rise of laser power (when the pulse first reaches peak power), and the power balance between inner and outer cones during the first and last phase. For the target, there are 3 parameters; the hohlraum length, capsule ablator thickness for fixed inside diameter, and capsule ablator mid-Z dopant fraction. The fifth and sixth columns show the expected initial and final 1 σ uncertainties in setting these parameters that are consistent with the uncertainties quoted for the four implosion parameters.

TUNING TECHNIQUES

Extensive sets of shots were completed at the Nova and Omega facility to demonstrate and downselect between proposed tuning techniques. The mainline tuning targets chosen are the high Z re-emission spheres [8] setting the foot cone power balance from the observed foot drive symmetry, liquid D₂-filled “keyhole” targets setting the laser power profile up to peak power from the observed shock speeds and overtake distances and times [9], streaked or gated x-ray backlit imploding capsules [10] setting the initial ablator thickness and peak laser power from the radiographically-inferred ablator mass remaining [11] and implosion velocity, and x-ray imaged imploded capsules setting the peak cone power balance and hohlraum length from observed core symmetry [12]. In addition, the soft x-ray power diagnostic “Dante” will be used to set the 4th rise launch time from the 4th rise slope and to set the ablator dopant fraction

from the measured hard (> 1.8 keV) x-ray preheat levels. The last two columns of Table I list the observables and their required tuning accuracy. The tuning accuracy requirements have been balanced in terms of uncertainty to mean ITF (typically set at $\pm 10\%$ for each term).

A. Drive Symmetry of First 2 ns

Ensuring spherical symmetry of the first shock launch is important for two reasons. First, simulations show that for an initial plausible 12% P_2 incident flux asymmetry averaged over the first 2 ns, the final ignition core asymmetry could be outside the requirement of $<10\%$ rms. Second, since shock timing is performed as a single point measurement (at the capsule equator, $\theta = 90^\circ$, see Section B), one must ensure that the measured first shock strength which sets 90% of the final compressed fuel entropy is representative of the solid angle averaged first shock strength. Based on these two considerations, the goal is to set the first 2 ns P_2 and P_4 drive asymmetry to 0 ± 5 and 7%, respectively. Since a 5% P_2 flux asymmetry over the first 2 ns would only lead to a few % ignition core asymmetry that could be masked or mistaken for other asymmetries later in the pulse, we needed a technique to isolate the first shock asymmetry. Two candidates, thin capsules that implode early [13] and backlit thinshells [14] that integrate the drive over shorter periods of time, were successfully tested and evaluated at Omega at 70% NIC-scale. Both have calculated undesirable heightened hydroinstability and shape distortion sensitivity to thickness non-uniformities since ensuring a relevant few ns bangtime requires starting with a much thinner 10- μm -shell. To record the instantaneous asymmetry during the first shock launch time (the first 2 ns), we have chosen instead to image the soft x-ray reemission from a non-imploding Bi ball [15] replacing the ignition capsule.

Figure 2a shows a schematic of the experimental set-up [8] at Omega used to validate the technique at NIC-relevant scale and Tr . Nearly identical diagnostic distances and parameters were used as for the planned NIC set-up. Also shown is an example of a re-emission image at $t = 0.7 \text{ ns}$, $h\nu = 900 \text{ eV}$ from a 1.4-mm diameter Bi sphere sampling a 100 eV, 1 ns drive in a 6.4-mm-long by 3.6-mm-diameter vacuum hohlraum irradiated by 21.4° and 59° Omega beams. Figure 2b shows the extracted P2 reemission asymmetry at $t = 0.7 \text{ ns}$ as a function of the imposed inner cone fraction showing the expected decrease in P2 with increased inner beam fraction. Since $h\nu/4k\text{Tr} \approx 3$, the $\pm 6\%$ accuracy in extracting a P2 asymmetry in the tail of a Planckian as shown in Fig. 2b translates to $\pm 2\%$ accuracy in inferred instantaneous incident P2 asymmetry, well within requirements. This accuracy is consistent with estimates based on shot noise and frame-to-frame variability. Recent experiments have extended the technique to full-scale (2.1 mm Bi ball in 9 by 5 mm hohlraum) and demonstrated the required accuracy for also inferring P4/P0.

B. Timing and Strength of First 3 Shocks

Ignition requires a pulse shape with a low power foot designed to send a carefully timed series of shocks through the frozen DT shell such that they overtake each other soon after they travel into the enclosed DT gas. If the shocks are too closely spaced, they will coalesce within the DT ice leading to an increase in the entropy at the inside surface of the DT ice, reducing compressibility. If they are too widely spaced, the DT ice decompresses between shocks. Since radiographic methods of assessing shock front velocities to the required 1-2% accuracies would require unrealistic sub- μm accuracy after accounting for the fuel compression that occurs after each shock passage, we opted for a direct continuous

measurement of the shock velocity. We achieve this by reflecting off the shock front [16] using a streaked 1D imaging laser-based interferometry system [17] “VISAR”, from which shock front velocities are extracted with the required 2-5% accuracy from fringe shifts and overtake distances extracted by integrating the velocity between time of first shock break-out from the ablator-fuel interface and time of next shock overtake seen as a sudden jump in fringe shift. The initial design [18] proposed a planar liquid D₂ cell sandwiched between the ablator and a transparent quartz window and placed on the side of the hohlraum to approximately mimic the DT ice drive conditions inside a capsule at the center of the hohlraum. Since then, with the realization that a 1 mm radius capsule provides an adequately large (>100 μm diameter) reflecting surface collected by the f/3 optics of the VISAR, the experimental design has evolved to using a liquid D₂-filled Au cone reentrant inside the capsule, greatly increasing the fidelity [19] of the drive conditions.

The viability of this tuning technique was successfully tested [9] in phases at Omega. First, we proved that the quartz window capping the liquid D₂ will not blank due to ionization from NIC-relevant levels of hard x-rays (> 2 keV) emanating from Au laser plasmas that can be transmitted through a surrogate ablator BeCu sample. Second, we demonstrated strong reflection off shock fronts traversing a NIC-scale liquid-D₂ filled cone equipped with a planar (rather than spherical due to limitations on hohlraum size at Omega power levels) BeCu ablator of matched areal density (see Figure 3). The hohlraum conditions were again designed to be a stringent test of window blanking by delivering up to 5x more M-band (> 2 keV) than expected during the third shock phase of NIF. We note that the other ignition capsule ablator designs, CH and HDC have about 2x the optical depth to these > 2 keV x-rays, and will be even less at risk of window blanking. Third, we demonstrated VISAR measurements off overtaking shots in the spherical converging geometry and shock strengths

of interest by switching to mm-scale directly-driven liquid D₂-filled CD capsules equipped with cones. Blanking of the D₂ was observed above third shock velocities (above 70 μm/ns), attributed to preheat from the shock front, further justifying the use of a different technique for monitoring the 4th shock as described in the next section.

C. Timing of 4th Shock

As for the second and third shocks, a correctly timed 4th shock (overtaking the first 3 shocks only after they have coalesced to ± 100 ps timing) is critical for keeping the fuel adiabat low for maximum compressibility. Too early a 4th shock will lead to 4th shock overtake in the fuel and an increase in entropy. In addition, too fast a 4th rise at any launch time leads to too strong a 4th shock and increased entropy. Finally, too late or long a 4th rise delays the onset of peak power and leads to poorer coupling of the main drive to the capsule since its surface area is continually shrinking after the first 3 shocks' passage, resulting in reduced implosion velocity at fixed peak power. Due to the VISAR window blanking at peak hohlraum drive levels, 4th pulse timing and strength has to be tuned from observing shock break-out time through an opaque witness plate [20] combined with a soft x-ray measurement of the 4th pulse rise of the hohlraum drive.

The viability of using the VISAR and SOP for this re-entrant witness plate shock breakout measurement was successfully tested [9] at Omega using the experimental set-up shown in Figure 4a. To test the system under the hard x-ray background expected at NIF at up to peak power, we drove the hohlraum to 230 eV over 1 ns, but with up to 12x more M-band x-rays than expect at peak power on NIF. A VISAR trace with superimposed self-emission typical of an SOP signature is shown in Figure 4b. While the VISAR signal is first lost due to hard

x-ray preheat-induced expansion for the thinner ($< 35 \mu\text{m}$) Au witness plates (at 4-5 ns), an abrupt rise (easily located to $\pm 25 \text{ ps}$) in optical signal upon thermal shock break-out is observed at later times. These experiments also showed that a sufficiently thick ($40\text{-}\mu\text{m}$) Au witness plate can delay significant preheat-induced expansion until after the thermal shock has broken out at a time in agreement with simulations. Moreover, calculations using the lower fraction of M-band preheat expected for NIF hohlraums due to lower beam intensities predict $20\text{-}\mu\text{m}$ -thick Au witness plates should be viable at NIF for ensuring the soft x-ray driven 4th shock breaks out before the preheat induced shock.

D. Ablator Mass Remaining and Implosion Velocity

For a given ignition design characterized by a peak laser power and laser energy, choice of hohlraum and capsule type and size, and initial assumptions on hohlraum and capsule coupling efficiency, there is an optimum setting for the combination of peak implosion velocity and amount of ablator mass remaining at implosion stagnation. An initially thin capsule can be driven to high implosion velocity in 1D, but per the rocket equation³, that leads to little residual ablator mass remaining, hence enhanced feed-through of Rayleigh-Taylor instability growth and eventually to DT fuel preheating by x-rays. An initially thicker capsule will be more immune to shell break-up by hydroinstabilities, but reach insufficient peak implosion velocity to provide enough PdV work to ignite the hotspot.

We elected to begin ablator tuning by streaked or gated x-ray radiography that will extract through Abel inversion the time-resolved ablator density profile from which remaining mass, areal density, position, and velocity of the ablator as a function of time can all be derived. The experimental set-up for NIC is shown in Fig 5. The capsule is identical to the ignition capsule

except for the 70 μm of DT ice replaced by an equivalent areal density of Be, 10- μm thick to maintain fidelity in its trajectory. The radiography source is an area backlighter in transmission mode created using 2 50° quads irradiating a 5-7 μm -thick backlighter foil (Ni He-alpha 7.8 keV for the BeCu design, Cu He-alpha 8.4 keV for the CH(Ge) and HDC designs) placed on the side of the hohlraum. 125- μm tall by 1.5-mm long slots are cut out of the hohlraum wall opposite each other to allow a fan of x-rays to backlight the capsule equator. They will be filled and encased in several 100 μm s of HDC to delay slot closure [21]. An experimental demonstration [10] of the streaked radiography technique on 0.5-mm-diameter graded-doped BeCu_{0.03} capsules driven by 200 eV, 2 ns-long shaped drives was completed at the Omega facility using a similar set-up as planned for NIF. The experiments were designed to check backlighter uniformity, sensitivity to thickness and to position of the Cu dopant which was even a greater contributor to the optical depth here due to the higher concentration of Cu required to approximate the same level of optical depth as for NIC with a smaller capsule. A typical streaked radiograph at the V He-alpha 5.4 keV line is shown in Figure 6a. The Abel-inverted analyzed results plotted in terms of pairs of measured peak velocities versus inferred ablator mass remaining are shown in Figure 6b for two different initial thickness capsules. Overplotted as squares are the Lasnex postshot calculations. We note that the statistical accuracy on its own met the $\pm 1\%$ of the initial mass requirement despite having 4-5x larger fraction of the mass remaining than expected for NIC implosions. In addition, Figure 6b shows that the data with the lowest statistical inaccuracy just met the $\pm 2\%$ peak implosion velocity accuracy (no in situ fiducial was used). Despite the scatter in the data for the nominally identical shots, it is promising to see that all the points follow the expected trend of less mass remaining if higher velocity.

By using symmetry capsules (discussed in Section E) at lower convergence with areal densities reaching < 0.2 g/cc, the spectra of D-³He 15 MeV burn protons [22] will also be used to corroborate the radiography measurements.

E. Peak Drive Symmetry

The time-integrated imploded core symmetry is mainly set by the drive symmetry during the peak power phase of the pulse. For example, a 0.4% applied P2 flux asymmetry will lead to a core asymmetry magnified by the (convergence ratio (CR) – 1), yielding a just acceptable 15% P2 asymmetry on the ignition capsule hot spot. As for the streaked convergent ablation measurement, the DT fuel is replaced by an equivalent areal density of pure Be to emulate the ignition capsule trajectory and hence drive symmetry history sampled.

The symmetry capsule became a robust technique for tuning both vacuum and gas-filled hohlraums in Nova hohlraums [2] where changing hohlraum length and/or beam pointing set the time-averaged single beam cone location near the P2 node. At Omega, the NIC concept of setting symmetry by balancing opposite sign P2 from different beam cones was first demonstrated [23] followed by rudimentary beam cone phasing [24]. The expected simultaneous improvements in P2 and P4 control [25] and associated implosion performance [26] followed. Recently, symmetry tuning at Omega has been extended to demonstrating sensitivity to cone fraction using small NIC-relevant case-to-capsule ratios of < 2.5 at Trs approaching 300 eV [12]. Figure 7a shows the experimental set-up and parameters for 260 eV, 1-ns-duration, 1.2-mm-diameter Omega hohlraums illuminated with 21° and 59° cones driving 560 μ m-diameter 45- μ m-thick CHGe.₀₂ capsules filled with a mixture of 36 atm. D2 + 3He. Figure 7b displays the > 4 keV 120- μ m-diameter core images recorded and the core P2

asymmetry extracted vs. 21.4° inner cone energy fraction for fixed total energy. The symmetry goes to more positive P2 as expected as the inner cone fraction is increased. In addition, a $\pm 1\%$ statistical accuracy in P2/P0 was demonstrated exceeding accuracy requirements for NIF capsules. The technique has been successfully ported to NIF in recent 500 kJ symmetry experiments, as shown in Fig. 8.

TUNING STRATEGY AND ACCURACY

The goals of the capsule tuning campaign are to specify the optimum adjustable parameter value and its uncertainty, and to assess that shot-to-shot variability is as expected. A cluster of N shots at a nominal laser and target setting would be taken to assess the 1σ shot-to-shot variability in the observable (to $\sigma/\sqrt{[2(N-1)]}$ accuracy) and compare to expectations. For the latter, the random measurement error bars must be and are expected from scaling from current technique demonstrations to be less than the data scatter. The second step is to correct the data for known preshot shot-to-shot target variations and postshot shot-to-shot laser variations, using calculated slope sensitivities to reduce the scatter in the data to just target and laser diagnostic metrology errors and errors in measuring the observable. In general, the mean of this corrected data will be offset from the optimum value of the observable we are aiming for, precorrected for any known surrogacy offset. The third step is to gather another set of M data points, where in general $M < N$ since data scatter has already been established, for another value of the adjustable parameter that would bracket the optimum setting. The optimum value of the adjustable parameter is then found by linear interpolation between the two datasets with a statistical accuracy = $\sigma/\sqrt{(M+N)}/\text{mean slope}$. Finally, one will have to add in quadrature systematic errors due to uncertainty in surrogacy, physics of the technique

and calibrations. The various contributions to the tuning accuracy for each of the adjustable laser and target parameters is shown in Figure 9 in terms of their variance normalized to the tuning budget [27] listed in the sixth column in Table I. Many of these terms are themselves rms sums of various contributors, to be discussed in a longer paper. Fig. 9 shows that we expect to meet the tuning accuracy budget for all parameters.

SUMMARY

A capsule performance optimization campaign will experimentally correct for residual uncertainties in the implosion and hohlraum physics used in our radiation-hydrodynamic computational models before proceeding to cryogenic-layered implosions and ignition attempts. The required tuning techniques have been shown experimentally and computationally to meet the required sensitivity and accuracy. The tuning campaign plans include checks of repeatability, iterations to overcome residual cross-couplings and contingency shots. A further set of in-flight capsule measurements are planned after the first ignition attempts if required isolating particular capsule physics issues. These include measuring Rayleigh-Taylor growth by x-ray radiography in convergent geometries (spherical or cylindrical), assessing the in-flight density differential between ablator and fuel (and hence the Atwood number and susceptibility to mix) using refraction-enhanced x-ray radiography [28], and measuring the in-flight fuel adiabat (essentially $1 +$ the ratio of T_e to the Fermi energy) by x-ray spectrally resolved Thomson scattering [29]. For the latter, recent experiments at Omega have demonstrated the feasibility of diagnosing imploding capsule conditions using the 9 keV Zn He-alpha resonance line.

*Work performed under the auspices of the Department of Energy by the Lawrence
Livermore National Laboratory under contract number W-7405-ENG-48.

REFERENCES

1. G.H. Miller, E.I. Moses and C.R. Wuest, Nucl. Fusion **44**, 228 (2004).
2. J. D. Lindl, P. Amendt, R. L. Berger, S. G. Glendinning, S. H. Glenzer, S.W. Haan, R. L. Kauffman, O. L. Landen, and L. J. Suter, Phys. Plasmas **11**, 339 (2004).
3. G.B. Zimmerman and W.L. Kruer, Comments Plasma Phys. Control. Fusion **2**, 51 (1975).
4. M. M. Marinak, G. D. Kerbel, N. A. Gentile, O. Jones, D. Munro, S. Pollaine, T. R. Dittrich, and S. W. Haan, Phys. Plasmas **8**, 2275 (2001).
5. T. C. Sangster, R. L. McCrory, V. N. Goncharov, D. R. Harding, S. J. Loucks, P. W. McKenty, D. D. Meyerhofer, S. Skupsky, B. Yaakobi, B. J. MacGowan, L. J. Atherton, B. A. Hammel, J. D. Lindl, E. I. Moses, J. L. Porter, M. E. Cuneo, M. K. Matzen, C. W. Barnes, J. C. Fernandez, D. C. Wilson, J. D. Kilkenny, T. P. Bernat, A. Nikroo, B. G. Logan, S. Yu, R. D. Petrasso, J. D. Sethian, and S. Obenschain, Nucl. Fusion **47**, S686 (2007).
6. D. S. Clark, S. W. Haan, and J. D. Salmonson, Phys. Plasmas **15**, 056305 (2008).
7. S. W. Haan, M. C. Herrmann, T. R. Dittrich, A. J. Fetterman, M. M. Marinak, D. H. Munro, S. M. Pollaine, J. D. Salmonson, G. L. Strobel, and L. J. Suter, Phys. Plasmas **12**, 056316 (2005).
8. E.L. Dewald, J. Milovich, J. Edwards, C. Thomas, R. Kirkwood, D. Meeker, O. Jones, N. Izumi, O.L. Landen, Rev. Sci. Instrum. **79**, 10E903 (2008).
9. T.R. Boehly, *et. al.*, Phys. Plasmas **16**, 056302 (2009).
10. D. Hicks, *et. al.* BAPS **53**, 2 (2008).
11. B. Spears, *et. al.*, J. Phys.: Conf. Ser. **112**, 022003 (2008).

12. G. Kyrala, *et. al.* BAPS **53**, 247 (2008).
13. N. M. Hoffman, D. C. Wilson and G. A. Kyrala, Rev. Sci. Instrum. 77 (10), 10E705-701-703 (2006).
14. R. K. Kirkwood, J. Milovich, D. K. Bradley, M. Schmitt, S. R. Goldman, D. H. Kalantar, D. Meeker, O. S. Jones, S. M. Pollaine, P. A. Amendt, E. Dewald, J. Edwards, O. L. Landen, and A. Nikroo, Phys. Plasmas **16**, 012702 (2009).
15. N. D. Delamater, G. R. Magelssen, and A. A. Hauer, Phys. Rev. E 53, 5240 (1996);
G. R. Magelssen, N. D. Delamater, E. L. Lindman, and A. A. Hauer, Phys. Rev. E **57**, 4663 (1998).
16. T. R. Boehly, D. G. Hicks, P. M. Celliers, T. J. B. Collins, R. Earley, J. H. Eggert, D. Jacobs-Perkins, S. J. Moon, E. Vianello, D. D. Meyerhofer, and G. W. Collins, Phys. Plasmas **11**, L49 (2004).
17. P. Celliers *et al.*, Rev. Sci. Instrum. **75**, 4916 (2004).
18. D.H. Munro
19. H. F. Robey, D H Munro, B K Spears, M M Marinak, O S Jones, M V Patel, S W Haan, J D Salmonson, O L Landen, T R Boehly and A Nikroo, J. Phys.: Conf. Ser. **112**, 022078 (2008).
20. R. L. Kauffman, L. J. Suter, C. B. Darrow, J. D. Kilkenny, H. N. Kornblum, D. S. Montgomery, D. W. Phillion, M. D. Rosen, A. R. Theissen, R. J. Wallace, and F. Ze, Phys. Rev. Lett. **73**, 2320 (1994).
21. A.B. Bullock, O.L. Landen, B.E. Blue, J. Edwards and D.K. Bradley, J. Appl. Phys. **100**, 043301 (2006).
22. D. C. Wilson *et al.*, Phys. Plasmas **5**, 1953 (1998).
23. T. J. Murphy, J. M. Wallace, N. D. Delamater et al., Phys. Rev. Lett. **81**, 78 (1998)

24. R. E. Turner, P. Amendt, O. L. Landen et al., *Phys. Plasmas* **7**, 333 (2000).
25. R.E. Turner, P.A. Amendt, O.L. Landen, L.J. Suter, R.J. Wallace, and B.A. Hammel, *Phys. Plasmas* **10**, 2429 (2003).
26. P.A. Amendt, R.E. Turner, and O. L. Landen, *Phys. Rev. Lett.* **89**, 165001 (2002).
27. S.W. Haan, *et al.*, *Eur. Phys. J. D* **44**, 249 (2007).
28. Jeffrey A. Koch, Otto L. Landen, Bernard J. Kozioziemski, Nobuhiko Izumi, Eduard L. Dewald, Jay D. Salmonson, and Bruce A. Hammel, *J. Appl. Phys.* **105**, 1 (2009).
29. H. Sawada, S. P. Regan, D. D. Meyerhofer, I. V. Igumenshchev, V. N. Goncharov, T. R. Boehly, R. Epstein, T. C. Sangster, V. A. Smalyuk, B. Yaakobi, G. Gregori, S. H. Glenzer and O. L. Landen, *Phys. Plasmas* **14**, 122703 (2007); Andrea L. Kritcher, Paul Neumayer, John Castor, Tilo Döppner, Roger W. Falcone, Otto L. Landen, Hae Ja Lee, Richard W. Lee, Edward C. Morse, Andrew Ng, Steve Pollaine, Dwight Price, Siegfried H. Glenzer, *Science* **322**, 69 (2008); H. J. Lee, P. Neumayer, J. Castor, T. Döppner, R. W. Falcone, C. Fortmann, B. A. Hammel, A. L. Kritcher, O. L. Landen, R. W. Lee, D. D. Meyerhofer, D. H. Munro, R. Redmer, S. P. Regan, S. Weber, and S. H. Glenzer, *Phys. Rev. Lett.* **102**, 115001 (2009).

TABLE I. Expected initial and residual post-tune 1σ offset from optimum ignition implosion performance, associated initial and post-tune 1σ offsets in optimal laser and target parameters, and required accuracy for tuning associated observables.

Implosion Performance Offsets			Laser or Target Offsets			Tuning Accuracy	
Parameter	Initial	Final	Parameter	Initial	Final	Observable	Value
DT Fuel	+10%	+3%	1 st 2ns Inner Cone	$\pm 25\%$	$\pm 10\%$	Reemit P2 flux	$\pm 15\%$
Adiabat			Energy Fraction			asymmetry	
Implosion Core	50%	15%	1 st 2ns Inner Cone	$\pm 25\%$	$\pm 10\%$	Reemit P2 flux	$\pm 15\%$
Asymmetry	rms	rms	Energy Fraction			asymmetry	
DT Fuel	+10%	+3%	1 st 2ns Laser	$\pm 20\%$	$\pm 10\%$	1 st Shock	$\pm 5\%$
Adiabat			Power			velocity	
DT Fuel	+10%	+3%	Trough Laser	$\pm 20\%$	$\pm 10\%$	1 st Shock	$\pm 5\%$
Adiabat			Power			velocity	
DT Fuel	+10%	+3%	2 nd Shock Laser	$\pm 10\%$	$\pm 4\%$	2 nd Shock	$\pm 2\%$
Adiabat			Power			velocity	
DT Fuel	+10%	+3%	3 rd Shock Laser	$\pm 10\%$	$\pm 4\%$	3 rd Shock	$\pm 2\%$
Adiabat			Power			velocity	
DT Fuel	+10%	+3%	2 nd Shock Launch	$\pm 200\text{ps}$	$\pm 50\text{ps}$	2 nd Shock	± 6
Adiabat			Time			overtake point	μm
DT Fuel	+10%	+3%	3 rd Shock Launch	$\pm 200\text{ps}$	$\pm 50\text{ps}$	3 rd Shock	± 6
Adiabat			Time			overtake point	μm
DT Fuel	+10%	+3%	4 th Shock Launch	± 200	± 100	4 th Shock	± 100
Adiabat			time	ps	ps	breakout time	ps
DT Fuel	+10%	+3%	4 th Rise Duration	$\pm 200\text{ps}$	$\pm 100\text{ps}$	4 th rise Tr slope	$\pm 5\%$
Adiabat						to peak power	
Ablator Mass	$\pm 80\%$	$\pm 25\%$	Initial Ablator	± 30	± 10	StreakCap Mass	$\pm 13\%$
Remaining			Thickness	μm	μm	Remaining	
Peak Implosion	$\pm 10\%$	$\pm 2\%$	Peak Laser Power	$\pm 20\%$	$\pm 4\%$	Velocity at r =	$\pm 2\%$
Velocity						300 μm	
Implosion Core	50%	16%	Peak Inner Cone	$\pm 20\%$	$\pm 5\%$	Symcap P2 core	± 7.5
Asymmetry	rms	rms	Energy Fraction			asymmetry	%
Implosion Core	50%	16%	Hohlraum Length	± 400	± 200	Symcap P4 core	± 7.5
Asymmetry	rms	rms		μm	μm	asymmetry	%
Ablator-fuel	$\pm 40\%$	$\pm 15\%$	Mid-Z Ablator	$\pm 0.3\%$	$\pm 0.1\%$	2-5 keV x-rays	$\pm 10\%$
Mix			Dopant Fraction			in hohlraum	
Peak Implosion	$\pm 10\%$	$\pm 2\%$	Peak Laser Power	$\pm 20\%$	$\pm 4\%$	Symcap	± 50
Velocity						Bangtime	ps

Figure Captions

Figure 1: Schematic of 16 laser and target parameters varied.

Figure 2. a) Re-emission sphere experimental set-up with example Omega data. b) P_2/P_0 of 900 eV x-ray emission from 2 mm diameter re-emission sphere versus inner cone fraction at 0.7 ns using NIC-relevant 1 cm long hohlraums and 100 eV drive.

Figure 3. a) 1st three shocks experimental set-up with example Omega VISAR data. b) Extracted velocity from VISAR trace of multiple shock directly-driven 1 mm diameter D₂ filled sphere equipped with re-entrant cone.

Figure 4. a) 4th rise experimental set-up with example Omega SOP data. b) Extracted break-out time from surrogate planar ablator driven by x-rays from NIC-relevant laser peak intensity ($\approx 10^{15}$ W/cm²).

Figure 5. Streaked capsule radiography experimental set-up for Omega shots.

Figure 6. a) Example of streaked 5.4 keV radiograph of 0.8 mm-diameter BeCu capsule driven by Omega 200 eV, 2.5 ns shaped drive hohlraum. b) Solid points are extracted peak implosion velocity versus % ablator mass remaining from 6 shots using 30 μ m (black) and 40 μ m (red) initial thickness graded doped BeCu shells. Open squares are postshot Lasnex simulations.

Figure 7. a) Symmetry capsule experimental set-up with example Omega data from 270 eV peak hohlraum drive. b) P_2/P_0 of 5 keV core x-ray emission shape from imploded 50 atm.-fill CH capsule versus inner cone fraction using NIC-relevant 270 eV peak drive.

Figure 8: Gated 8-10 keV x-ray images of convergence ratio 15 CH capsules driven by 500 kJ 270 eV peak temperature NIF hohlraums.

Figure 9. Illustrative example of how a number of shots measuring ablator mass remaining will be used to check variability and to set the optimum associated target parameter, the initial ablator thickness, and its 1 sigma uncertainty.

Figure 10: Residual variances after tuning in random measurement error, systematic errors, target metrology errors, and laser diagnostic errors normalized to budget for each of the laser and target adjustable parameters.

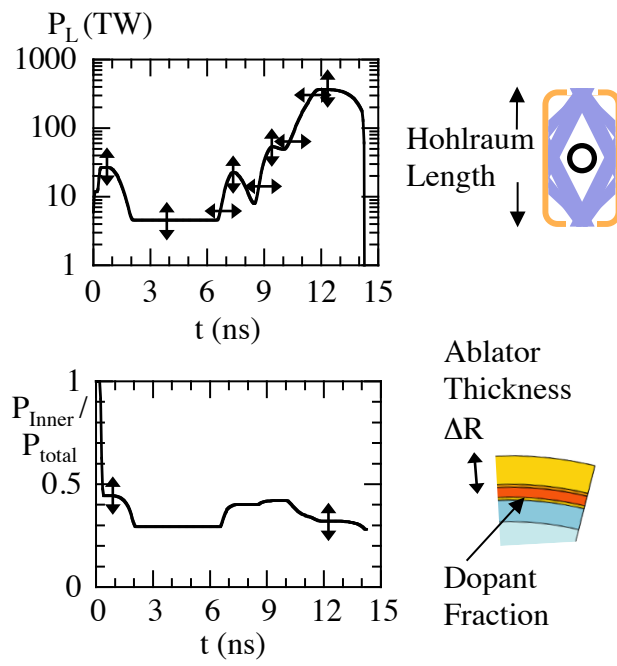


Figure 1

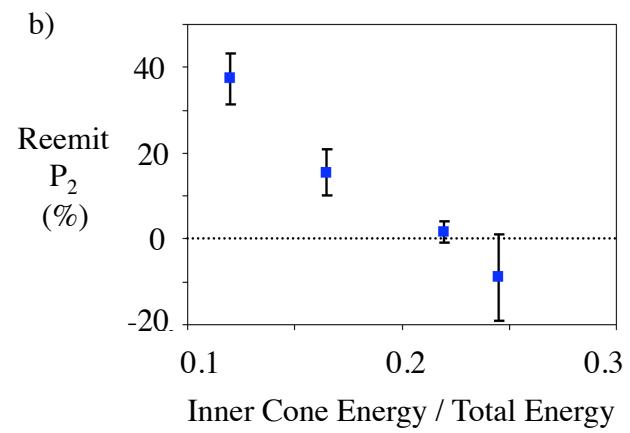
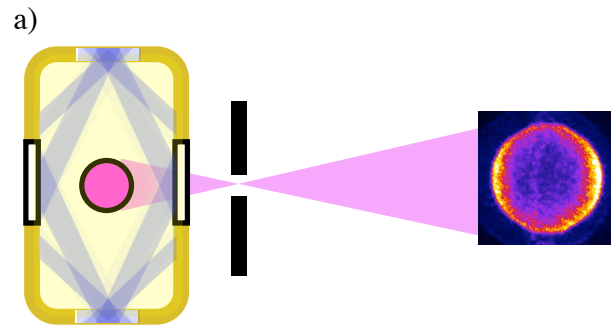


Figure 2

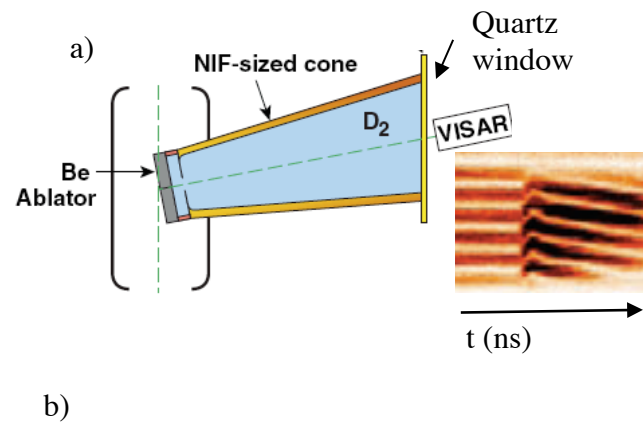


Figure 3

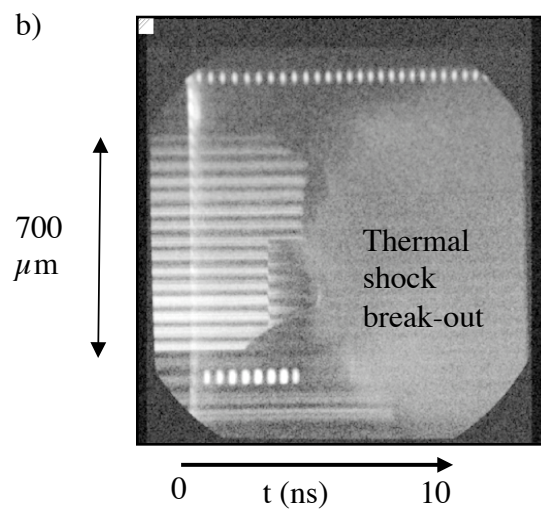
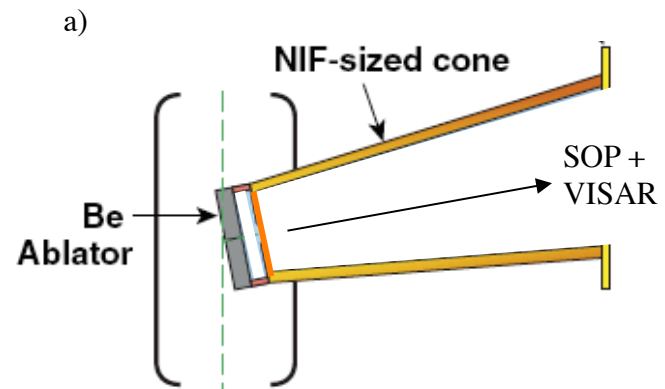


Figure 4

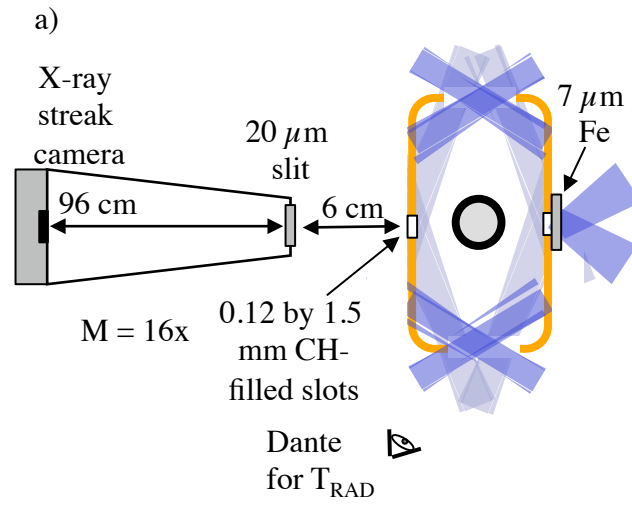
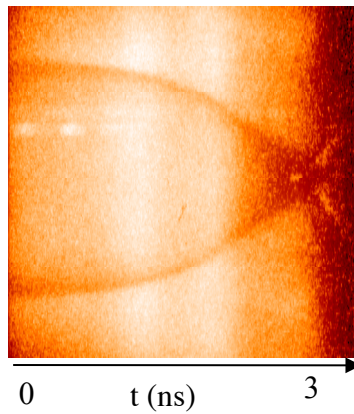
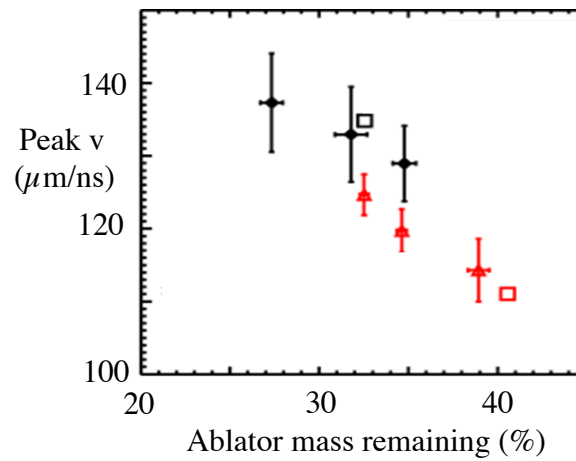


Figure 5

a)



b)



Add analytic
scalings

Figure 6

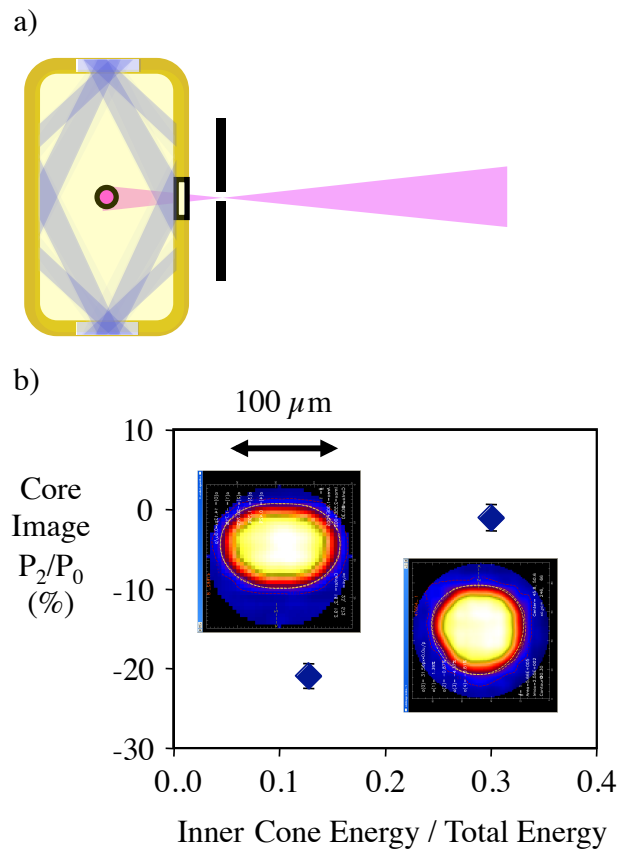


Figure 7

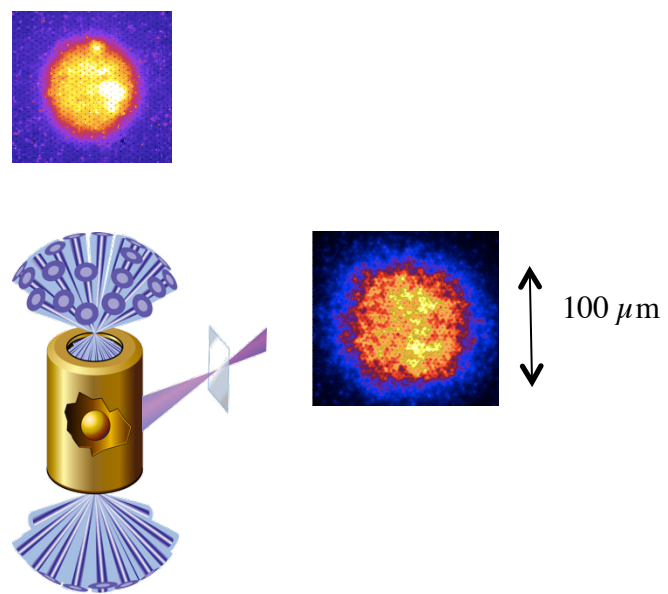


Figure 8

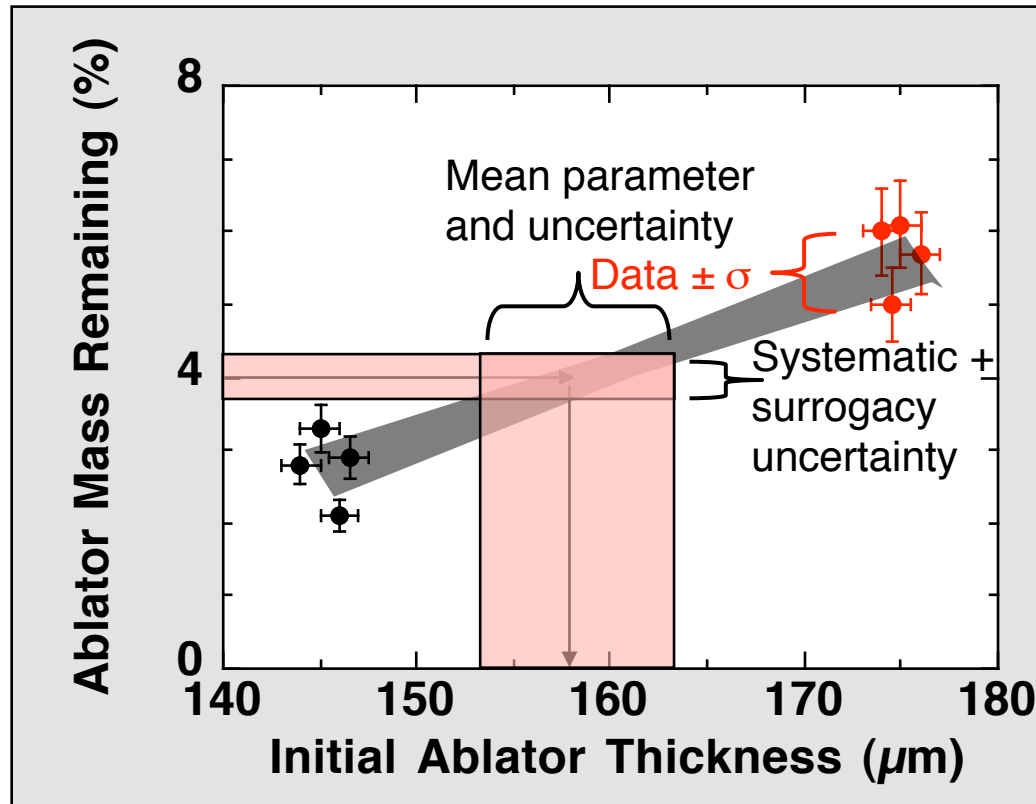


Figure 9

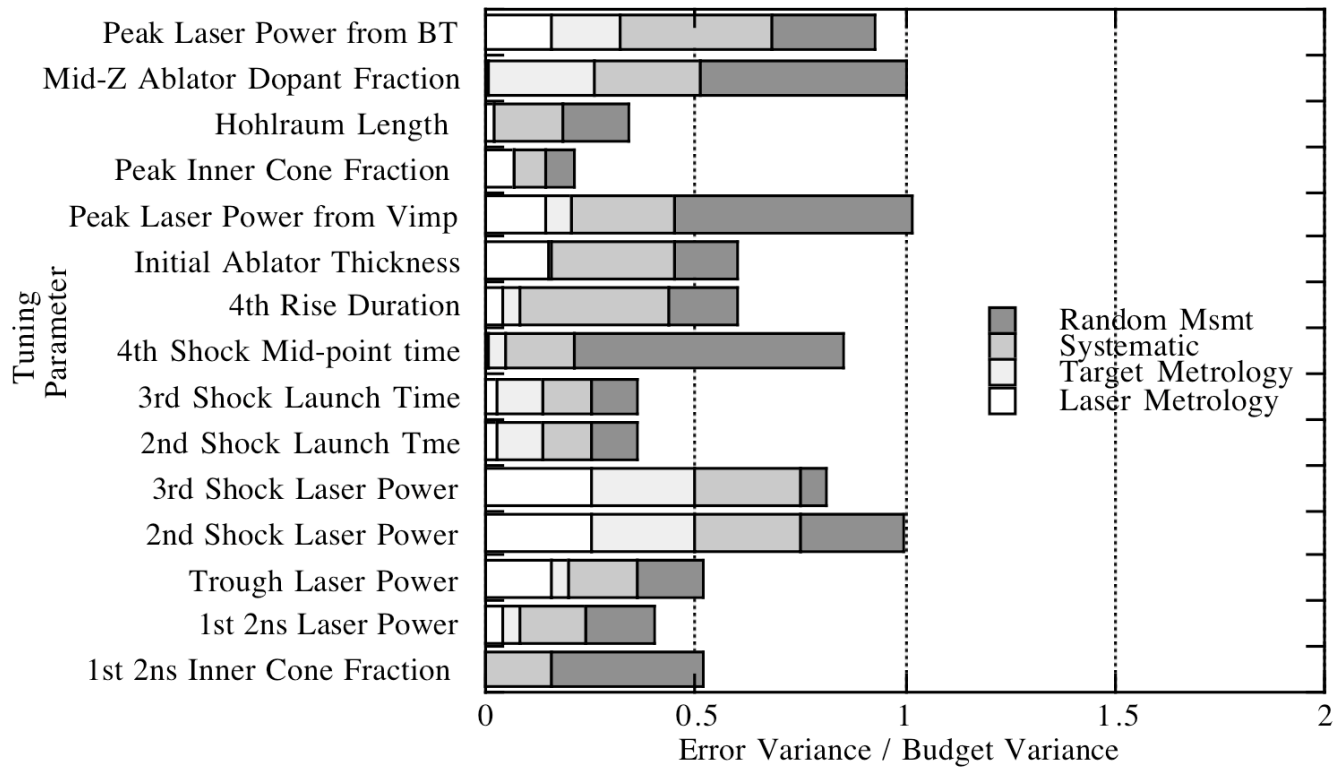


Figure 10